https://doi.org/10.5194/egusphere-2026-5184
Preprint. Discussion started: 10 September 2026

Recent cooling of Atlantic Intermediate Waters in Kangertittivaq (Scoresby Sund) driven by large-scale advection and a glacial meltwater plume

Torsten Kanzow[1,2], Rebecca McPherson[1], Claudia Wekerle[1], Wilken-Jon von Appen[1], Oliver Huhn[2], Donald Slater[3], and Andreas Münchow[1]

[1]Alfred Wegener Institute, Helmholtz Centre for Polar and Marine Research, Bremerhaven, Germany
[2]Faculty of Physics, University of Bremen, Bremen, Germany
[3]School of Geosciences, University of Edinburgh, Edinburgh, UK

Correspondence: Torsten Kanzow (Torsten.Kanzow@awi.de)

Abstract. Ocean heat transport to marine terminating glaciers in Greenland exhibits interannual variability whose drivers remain incompletely understood. Using 2016-24 observations from Kangertittivaq, Greenland's largest fjord system, we show that Atlantic Intermediate Water (AIW) that enters the fjord undergoes cooling throughout the fjord on interannual time scales, driven by advection of waters from the West Spitsbergen Current in Fram Strait. The strength of the subsurface inflow into Kangertertivarmît Kangertivat, the largest inner fjord branch, depicts distinct maxima in summertime, likely driven by entrainment of AIW into the meltwater plume of Daugaard-Jensen Glacier. Our study thus reveals that a superposition of large-scale advection and fjord meltwater dynamics facilitates the AIW cooling in the entire fjord system. We show that Kangertittivaq exhibits the same major AIW cooling event as 79N Glacier located 1000 km farther north, pointing to a common basin-scale forcing, synchronising ocean thermal conditions across a broad sector of the Greenland margin.

1 Introduction

The interaction between ocean and marine-terminating glaciers depends on both oceanic and glacial influences — such as the supply of warm ocean waters, the input of meltwater, and iceberg calving. The significance of these influences varies from region to region and from fjord to fjord (Slater and Straneo, 2022). One such deep fjord is Kangertittivaq (Scoresby Sund) which represents Greenland's largest fjord system hosting several marine terminating glaciers (Fig. 1). Kangertittivaq consists of an outer region about 30 km wide at the fjord's mouth near 22°W. West of 25°W it branches into several narrow and deep fjords. The longest of them is Kangertertivarmît Kangertivat (Nordvestfjord; hereafter referred to as KK), at the head of which we find its most active glacier, Daugaard-Jensen Glacier (Dowdeswell et al., 2016). It constitutes a major source of icebergs in East Greenland (Dowdeswell et al., 1993), discharging roughly 10 Gt a^{-1} into the fjord (Mouginot et al., 2019; Mankoff et al., 2020b). Water depths reach 500 m in the wide outer part of Kangertittivaq, while exceeding 1000 m in KK. Throughout the entire fjord system, we find Atlantic Intermediate Water (AIW) with temperatures higher than 0.5°C below 300 m depth (Fig.

https://doi.org/10.5194/egusphere-2026-5184
Preprint. Discussion started: 10 September 2026

1; Seifert et al. (2019); hereafter S19). A layer of colder and fresher Polar Water (PW) dominates the upper layer with minimal temperature less than -1°C, thinning from the fjord mouth towards its head in KK.

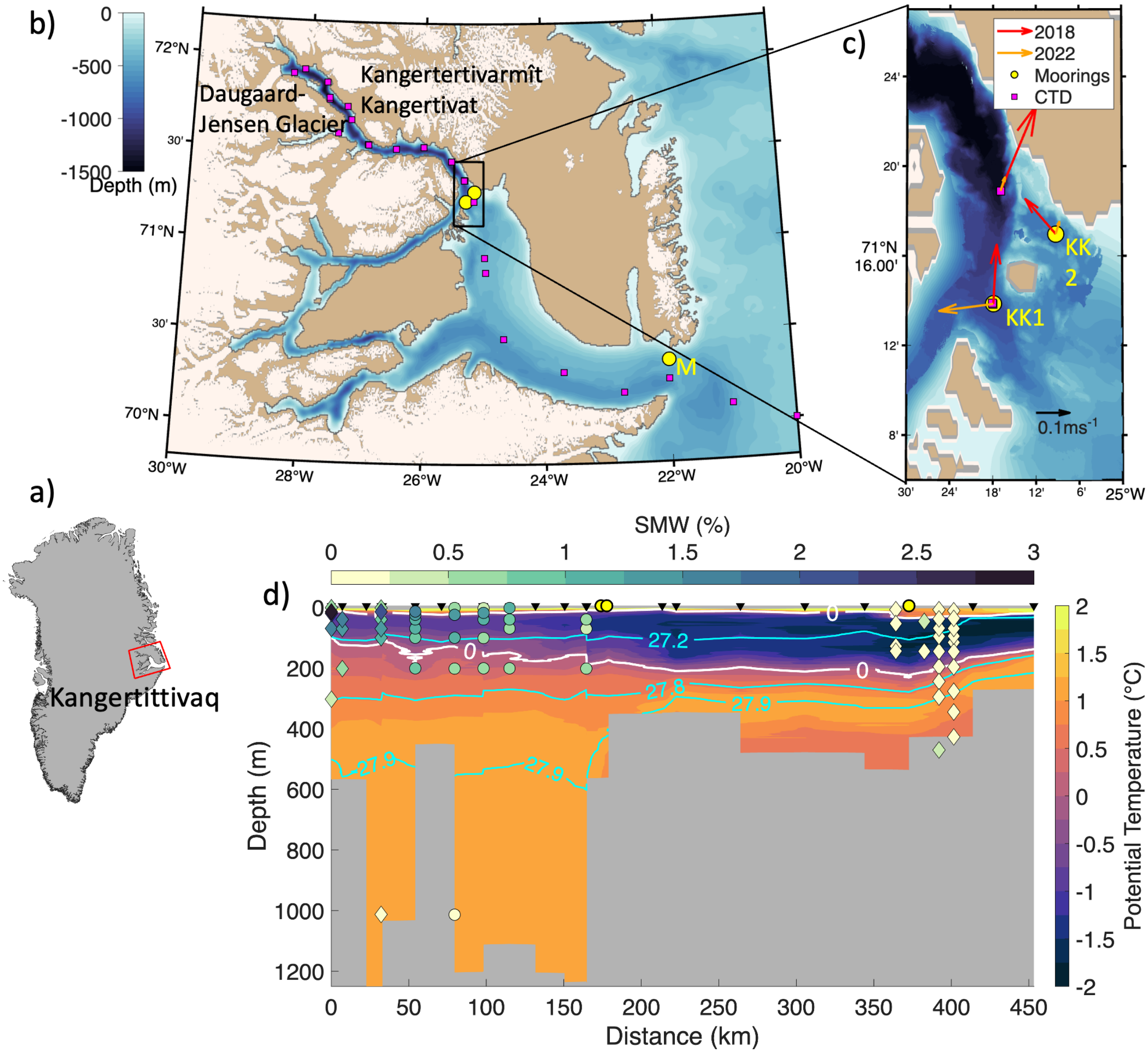

Figure 1. Maps of (a) Greenland and (b) Kangertittivaq with measurement locations of the MSM76 expedition (moorings in yellow; CTD stations in magenta). (c) KK entrance area with high-resolution bathymetry (courtesy of Alfred-Wegener-Institute). Arrows show near-bottom currents from LADCP profiles in 2018 (red, MSM76) and 2022 (orange, PS131). (d) Along-fjord distribution of potential temperature between fjord head in KK (left) and outer Kangertittivaq (right) based on data from S19. White and cyan lines show the 0°C isotherm and isopycnals, respectively. Overlaid are submarine meltwater fractions measured in 2016 (MSM56, circles) and 2019 (MSM85, diamonds).

S19 has been one of the first studies to focus on the oceanography of Kangertittivaq. It revealed that waters from the Greenland continental shelf flow into the fjord across the northern part of the fjord mouth below 100 m depth, with return flow

https://doi.org/10.5194/egusphere-2026-5184
Preprint. Discussion started: 10 September 2026

occurring in the southern part of the mouth at depth. A similar cyclonic exchange flow at the fjord mouth may also be present in the surface waters (Digby, 1953). This horizontal exchange flow may arise because the local internal Rossby radius of 6 km is small relative to the 30 km wide fjord entrance (S19). In contrast, at the entrance from the outer sound to KK (hereafter referred to as KK entrance) the fjord narrows, the seafloor steeply descends (Fig. 1c), and a bottom-intensified upfjord flow of warmer saltier AIW compensates a seaward flow of colder fresher waters above, thus featuring an estuarine-type circulation. As S19 relies on summertime hydrographic and velocity surveys, it remains uncertain if the results are representative of annual mean conditions.

It is known that other deep glacial fjords in east Greenland exhibit significant interannual changes of AIW properties. In the case of the Nioghalvfjerdsfjorden (79N Glacier) in the far northeast of Greenland, the floating ice tongue has thinned by around one third from 1998 to 2016 (Mayer et al., 2018). Wekerle et al. (2024) showed that a multi-decadal increase of the heat supply by AIW from the shelf of Northeast Greenland dominated glacier melt over the past decades. Schaffer et al. (2017) revealed that the AIW warmed from the time period 1979–1999 to 2000–2016 by 0.5°C on the shelf near the 79N Glacier and Zachariae Isstrøm, while this warming was traced back to the West Spitsbergen Current in eastern Fram Strait (McPherson et al., 2023). Gjelstrup et al. (2022) showed that the long-term increase of both AIW temperature and layer thickness extended across the entire shelf of NE Greenland north of Denmark Strait. Recently, Heide-Jørgensen et al. (2026) concludes that AIW temperatures outside of Kangertittivaq (in Blosseville Basin and along the Blosseville coast) had experienced a longterm warming of 0.5 – 1.0°C between the 1960s and 2016. Contrary to the observed long-term warming, McPherson et al. (2024) realized that AIW temperatures at the 79N Glacier cooled by 0.65°C between 2018 and 2021 and thus reduced submarine glacial melt. This cooling, too, could be traced to similar changes of Atlantic Water upstream in the West Spitsbergen Current about 2 years prior.

Given the large distance of 300 km between the fjord mouth of Kangertittivaq and the Daugaard-Jensen Glacier at the head of the fjord, it is unclear to which extent the glacier is exposed to the AIW variability on the Greenland shelf. Wood et al. (2024) conclude from numerical simulations that increasing submarine melt rates driven by subsurface ocean warming triggered the retreat of the Daugaard-Jensen Glacier after 2010. This study is thus timely in that it investigates the temporal AIW variability within Kangertittivaq using 2018 to 2022 time series measurements combined with summertime hydrographic surveys between 2016 and 2024. We interpret the AIW variabilty in the framework of both advection from the open ocean and local forcing near the fjord mouth as well as inside of Kangertittivaq.

2 Methods

2.1 Data

We deployed and recovered three moorings, namely KK1, KK2, and M, in August 2018 and 2022 during the expeditions MSM76 (Kanzow et al., 2020) and PS131 (Kanzow, 2023) respectively, measuring temperature salinity and velocity. Mooring M was placed at the mouth of the fjord in the pathway of the subsurface AIW inflow (S19) while moorings KK1 and KK2 were

https://doi.org/10.5194/egusphere-2026-5184
Preprint. Discussion started: 10 September 2026

located near the KK entrance to determine the flow structure and its variability towards the Daugaard-Jensen Glacier (Fig. 1). We list details in Table 1.

Expeditions in the summers of 2016 (S19), 2018, and 2022 included hydrographic (CTD) profiles in Kangertittivaq using a SBE 911-plus system. The salinity profiles were calibrated at sea using salinometry with standard reference water samples. We also used data from airborne XCTD probes in Kangertittivaq and on the shelf off Greenland acquired between 2016 and 2021 by NASA's OMG program (OMG, 2016; Fenty et al., 2016). One CTD profile (fjord mouth; August 2024) was provided by the Greenland Climate Research Center.

To compare the water masses at the fjord mouth with hydrographic properties in the Nordic Seas, all available quality-controlled, delayed-mode Argo float profiles obtained in the Greenland Sea offshore Kangertittivaq between March 2015 and March 2022 were used (Argo, 2000). The monthly-mean Atlantic Water temperature timeseries from the West Spitsbergen Current mooring array (1997–2024) in eastern Fram Strait was obtained from McPherson et al. (2026). The noble gas (He and Ne) data obtained in 2016 during MSM56 and in 2019 during MSM85 were measured at IUP Bremen noble gas mass spectrometry lab (Sültenfuß et al., 2009). The derivation of submarine meltwater fraction from He and Ne is described below.

Table 1. Details of the moorings deployed in Kangertittivaq and Norske Trough, including sensor depths, sampling rate and specific comments.

Site	Sensor	Depth (m)	Sampling rate (d^{-1})	Variables	End of record
KK1	AA RCM11	410	12	T,u,v	10/08/2022
KK1	SBE-16	610	24	T,S,P	10/08/2022; S flawed
KK2	RDI ADCP 75 KHz	796	12/0.1760[1]	u,v,T	11/7/2022
KK2	SBE-16	800	24	T,P	10/8/2022 (T);S flawed
M	SBE-16	250	24	T,S,P	11/8/2022 (T);04/1/2020 (S)
M	SBE-37	300	144	T,S,P	26/6/2019
M	SBE-56	330	4320	T	24/7/2021
IdF	SBE-37	152	144	T,S,P	07/10/2025
IdF	SBE-37	292	144	T,S,P	07/10/2025
IdF	SBE-37	356	144	T,S,P	07/10/2025

[1] Before/after 26/10/2018.

2.2 Mooring data processing

The moorings M, KK1 and KK2 contained sensors to measure temperature (SBE56), conductivity-temperature-pressure (CTD; SBE37 and SBE16), and velocity (RDI 75 KHz ADCP in KK2, Aanderaa RCM11 in KK1). In order to fill data gaps and eliminate time-variable mooring motion, the eastward and northward velocity components from the ADCP at site KK2 were interpolated onto a fixed depth grid of 8 m resolution. The preset sampling rate of the ADCP had been 2 hours. After 26 Oct, 2018, the resolution of the recorded measurements abruptly switched from 2 hours to roughly 5.7 days for reasons unknown.

https://doi.org/10.5194/egusphere-2026-5184
Preprint. Discussion started: 10 September 2026

The fact that the temperature recorded by the ADCP showed a correlation exceeding 0.96 to that of a temperature record from a SBE-16 sensor placed 4 m below the ADCP, however, convinced us that the time stamps of the ADCP can be trusted throughout the entire deployment period. The ADCP data were interpolated on a 12-hour time grid and subsequently low-pass filtered using a 48-hours cutoff (recursive 5th Butterworth filter). Both the coarse temporal sampling resolution and our crude data treatment might cause tidal aliasing to be present in the processed record, yet the uncontaminated part of record before 26 Oct, 2018 reveals tidal peaks not exceeding O(4 cm/s), which are small compared to the seasonal peak velocities, as will be shown. A rotation of the east-north coordinate system was performed, with the velocity component reported here corresponding to the direction of maximum time mean velocity near the sea floor (with positive values representing inflow into Kangertertivarmît Kangertivat).

The mooring temperature, salinity and pressure data were collected every 2 hours, then 2-day low-pass filtered (recursive 5th order Butterworth filter) and gridded onto a regular 12 hours time grid. The SBE-16 salinity records from sites KK1 and KK2 showed jumps and large drifts early on in the records and were excluded from the analysis. The SBE-37-based salinity record at M is unsuspicious however only the first ten months are available before the recording stopped prematurely. The SBE-16 salinity record at M appears clean until early January 2020 (when comparing it in T/S space with the SBE-37 record from the same mooring). Values from this device after January 2020 were excluded from the analysis. The SBE-37 records from mooring IdF (deployed at 78°10.7'N and 015°43.1'W) are all complete and clean throughout the entire deployment. Table 1 provides additional detailed information on mooring deployment and sensors.

2.3 Extension of AIW temperature time series at 79N Glacier until 2025

We aim at comparing the evolution of the AIW temperatures in Kangertittivaq with that close to the 79N Glacier (Nioghalvfjerdsfjorden Glacier) located roughly 1000 km north. For this purpose, we use the AIW temperature time series obtained right at the calving front obtained by Schaffer et al. (2020) for the mid-2016 to mid-2017 period and extended until mid-2021 by McPherson et al. (2024). In order to extend the time series to mid-2025 (when no mooring was deployed at the calving front), we made use of mooring IdF deployed in Norske Trough near the island Ile-de-France (IdF, 78°10,73'N, 015°43,12'W), purposefully located in the flow pathway of AIW from the continental slope toward the 79N Glacier (Schaffer et al., 2017; Münchow et al., 2020) and deployed between July 2022 and October 2025. In order to make the AIW time series at IdF comparable to the one at 79N Glacier located ≈ 150 km downstream, we interpolated the IdF temperatures from the three CTD sensors (see Table 1) onto the potential density surface of $27.80\ \mathrm{kg\ m^{-3}}$. This density is in good agreement to the density of the near-bottom inflow of AIW into the cavity below the floating ice tongue of the 79N Glacier (Schaffer et al., 2020).

2.4 Meltwater fractions

Atmospheric air with a constant composition of the noble gases He and Ne is trapped in the ice matrix during formation of the meteoric ice. When the ice is melting at depth or at the ice shelf base inside an ice shelf cavity, these gases are completely dissolved in the water due to the enhanced hydrostatic pressure. This leads to an excess of ΔHe = 1280 % and ΔNe = 890 % in pure submarine meltwater (SMW) compared to the air-water solubility equilibrium (Loose and Jenkins, 2014). Melting at the glacier or ice shelf surface would equilibrate quickly with the atmosphere and does not show a significant noble gas excess in ocean water (the calculated excess of 100% surface melt water amounts to max. 23% for He and 27% for Ne due to the salinity of zero at 0°C compared to ocean water with a salinity of e.g. 34.5 at 0°C).

Here, SMW refers to all water melted not at the surface, namely comprising meltwater from the underside of a floating ice tongue, from a glacial front at depth, and from melt occurring upstream of the grounding line by friction or geothermal heat. Surface meltwater penetrating through the glacier and being discharged into the ocean at the grounding line (often referenced as subglacial runoff), is not detected by our method.

To calculate the SMW fraction in each sample from He and Ne, we use the method from Rhein et al. (2018) and Huhn et al. (2021). Firstly, to exclude the natural oversaturation that is notorious almost everywhere in ocean water (Loose and Jenkins, 2014), the mean noble gas excess in the mixed layer ($\Delta C_{surf-excess}$) far away from the source is subtracted from all measured values. For the MSM56 noble gas data, as no stations outside the fjord and away from the glacial sources were available, we used data from the expedition MSM43 off the continental slope of East Greenland taken within 20 m from the sea surface. We found $\Delta He_{surf-excess}$ = 5.0 ± 0.6 % and $\Delta Ne_{surf-excess}$ = 4.2 ± 0.6 %.

Secondly, we subtracted the equilibrium value from each sample using the solubility function $Ceq = f(T,S)$ from Weiss (1971). Third, the remaining concentration is finally attributed to the presence of pure SMW with He = 26.189 nmol/kg and Ne = 88.739 nmol/kg (Beaird et al., 2015). The uncertainties of mean $\Delta C_{surf-excess}$ results in an error of SMW of 0.06-0.09 % using He and ± 0.07-0.09 % using Ne. The measurement error of ± 0.4 % for both He and Ne result in an error of SMW of 0.03 %. The total uncertainties then amount to SMW(He) ± 0.1 % and SMW(Ne) ± 0.1 %. SMW fractions $\geq 0.1\%$ are assumed to be significant.

2.5 Models

We use the buoyant plume model of Slater et al. (2016) to diagnose entrainment of ambient waters into the plume driven by subglacial discharge at Daugaard-Jensen glacier. Forcing this model, we use 10-day lagged estimated subglacial discharge from RACMO (Mankoff et al., 2020a). The time lag accounts for the delay between surface runoff generation and its arrival at the glacier's grounding line. Moreover, we use ambient hydrographic profiles from the summer 2016 survey (S19), a grounding line depth of 748 m from Bedmachine (Morlighem, 2022), and assume a plume width of 200 m. Weak subglacial discharge in winter is included to account for basal melt produced by the ice sheet, following Karlsson et al. (2021).

To analyze the large scale variability of AIW in the Nordic Seas and at the mouth of Kangertittivaq, we used output of the ocean model FESOM2 (Danilov et al., 2017). Our configuration is specific for Northeast Greenland (Wekerle et al., 2024), i.e., the unstructured global mesh is refined to 4.5 km in the Nordic Seas and Arctic Ocean including Kangertittivaq. The simulation covers the period 1960–2021 and is forced by atmospheric reanalysis data from JRA55-do (Tsujino et al., 2018) which also includes global river runoff. For Greenland, the river runoff has been replaced with liquid and solid runoff from Mankoff et al. (2020a) and Mankoff et al. (2020b).

https://doi.org/10.5194/egusphere-2026-5184
Preprint. Discussion started: 10 September 2026

3 Results

3.1 Spatially coherent interannual AIW variability in the fjord

Variability in AIW temperatures is revealed by hydrographic profiles taken near the mouth of Kangertittivaq during the summers of 2016, 2017, 2018, 2020 and 2022 (Fig. 2a). In 2016, maximum AIW temperatures are only about 1.2°C, whereas the AIW maximum in 2017 and 2018 reach 1.6°C. By 2022, temperatures return to and subsequently remain at levels similar to those in 2016 (Fig. 2a). Mooring-based temperature time series from 2018 to 2022 at the fjord mouth reveal pronounced seasonal variability with annual amplitudes exceeding 0.7°C at a depth of 250 m (Fig. 3a, black line). This 4-year time series also exhibits an interannual cooling trend with 2022 being about 0.5°C cooler than 2018. This observation is consistent with the cooling we observe in the summer-only hydrographic profiles (Fig. 2a). Furthermore, the 3-years-long time series at 330 m depth also exhibits a smaller cooling trend from 2018 to 2021.

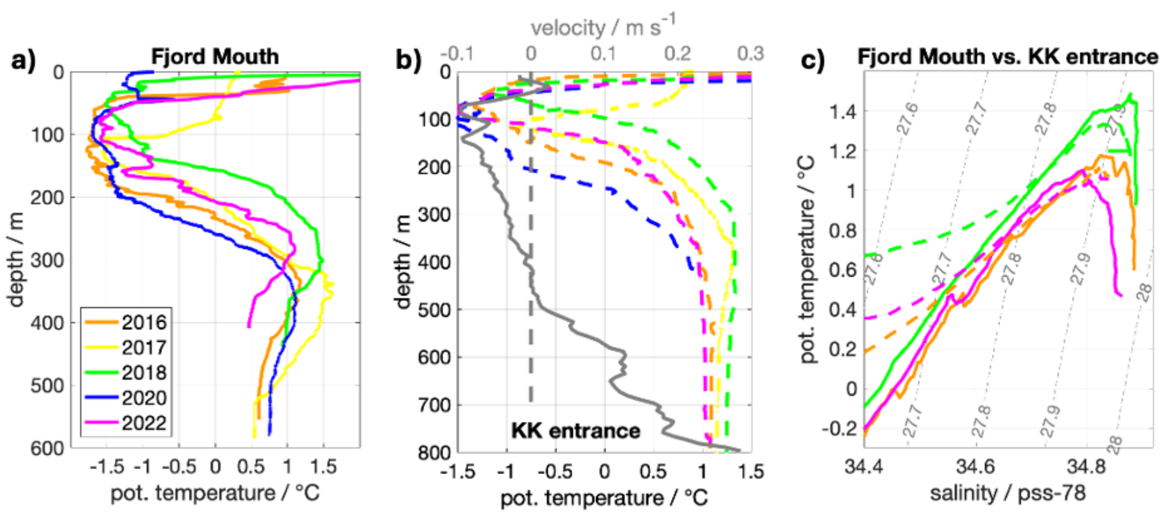

Figure 2. Temperature profiles (a) near the fjord mouth and (b) at KK entrance. Panel (b) includes current velocity from an LADCP profile (positive values denote inflow into KK) obtained in August 2018, co-located with the CTD measurements. Panel c) shows T/S diagrams of profiles from 2016, 2018 and 2022, with solid and dashed lines representing the fjord mouth and KK entrance, respectively.

We investigate next how these changes extend into the fjord towards Daugaard-Jensen Glacier. At the KK entrance, hydrographic profiles reveal a similar pattern of AIW maximum temperatures of about 1.1°C in 2016, an increase to 1.3 °C in 2017 and 2018, and returning to 2016 levels in 2020 and 2022 (Fig. 2b, c). The mooring-based temperature records within the AIW layer at the KK entrance show substantial variation (Fig. 3c). The bottom-most sensor at 800 m depth exhibits a rapid temper-

https://doi.org/10.5194/egusphere-2026-5184
Preprint. Discussion started: 10 September 2026

ature drop exceeding 0.3°C in mid-2019 with a slow subsequent return to prior values. Similarly, sensors located 200 m above the seafloor show an even sharper decline in 2019 of 0.5°C, followed by a subsequent increase. The temperature drop is nearly density-compensated, as shown by the alignment of temperature maxima in Fig. 2c along a single isopycnal. In summary, all records reveal a sudden cooling of AIW of roughly 0.3-0.5°C within less than 3 months in early 2019.

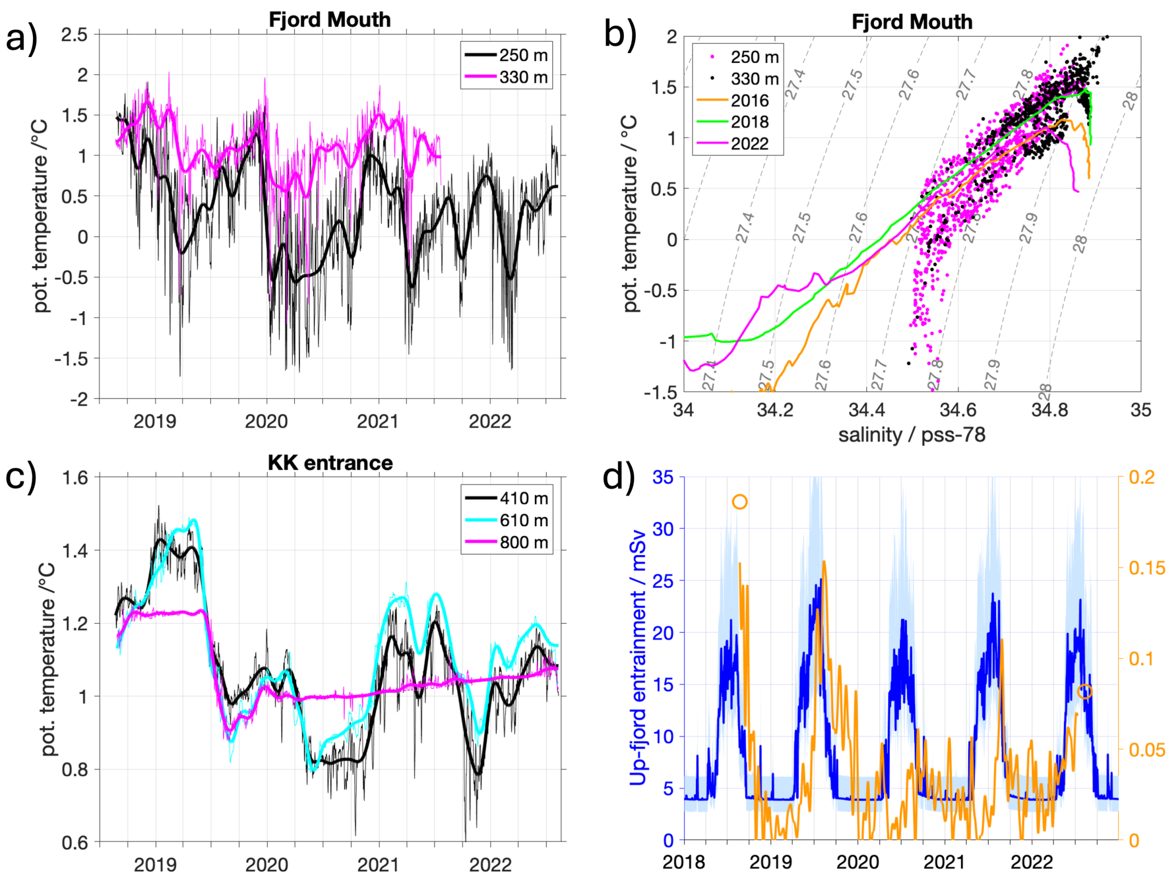

Figure 3. (a) Time series of temperature at the fjord mouth (mooring M) at 250 and 330 m depth (2-day and 60-day low-pass filtered). (b) T/S diagram from time series shown in panel (a) (magenta and black dots), and from profiles at the fjord mouth from summers of 2016, 2018 and 2022 (solid lines). (c) Time series of temperature at KK entrance (moorings KK1 and KK2) at 410, 610 and 800 m depth (2-day and 60-day low-pass filtered). (d) Time series of 15-days low-pass filtered ADCP-based inflow velocity (averaged over the bottom-most 200 m) into KK at site KK2 (orange line). Orange circles denote average velocity from 3 LADCP profiles near site KK2 averaged over the bottom-most 200 m in August 2018 and 2022. The blue line shows simulated entrainment of AIW into the meltwater plume of Daugaard-Jensen Glacier assuming a plume width of 200 m, including a light blue sensitivity envelope (for plume widths between 100 and 500 m).

In addition to the cooling AIW trends both at the fjord mouth and KK entrance, Fig. 2c suggests that the temperature-salinity patterns of both areas vary in unison. In 2018 we find a pronounced AIW peak at both sites, while in 2016 and 2022 consistently

https://doi.org/10.5194/egusphere-2026-5184
Preprint. Discussion started: 10 September 2026

colder and less saline AIW maxima emerge. We conclude that AIW properties between the fjord mouth and KK entrance are correlated at interannual time scales. We posit this phenomenon to be driven by advection of AIW from the East Greenland shelf into the fjord, and will return to this observation below.

3.2 Seasonal hydrographic change at the fjord mouth

Both interannual and seasonal forcing control the flow and temperature of AIW into the fjord. Our mooring records at the entrance of the fjord reveal significant temporal variability of temperature (Fig. 3a). At 250 m depth (slightly above the AIW temperature maximum), we find summertime values of about 1.0°C and subsequently cooling each year in winter with short term events repeatedly displaying values less than -1.0°C. The amplitude of the low-frequency seasonal cooling reaches about 1.5°C (Fig. 3a). At 330 m depth (below the AIW maximum), we occasionally observe wintertime temperatures as low as 0.0°C though in contrast, summertime temperatures at this depth reach 1.5°C. The seasonal cooling amplitude at 330 m is 0.7°C (or half of the at 250 m amplitude).

The winter T/S characteristics at the fjord mouth depart from those in summer (Fig. 3b), with a saline but cold water mass temporarily replacing the warmer AIW. This water mass must originate from outside of the fjord because we do not find waters with similar properties within it. Strong vertical stratification of Greenland's coastal waters generally prevents local convection. Thus either advection within the East Greenland Current from the north along the shelf break, or an inflow from the open ocean to the east (Blosseville Basin) remain as possible sources. Argo float-based CTD profiles (Fig. 4) reveal two offshore areas where T/S characteristics appear similar to the wintertime conditions we find at the fjord mouth (salinities between 34.4 and 34.6 and temperatures smaller than -1.0°C). The first location is found in Blosseville Basin (the western Iceland Sea) close to where a topographic depression connects the fjord with the shelf break, and the second we identify in the Greenland Sea north of 71°N seaward of the shelf break. Because the occurrences of such cold and saline waters are rare along the East Greenland Current pathway to the north of the entrance to Kangerittivaq, it seems more plausible that wintertime properties at the fjord mouth originate from Blosseville Basin.

3.3 Seasonal AIW inflow into Kangertertivarmît Kangertivat driven by buoyant plume

Though time series of velocity measurements at the fjord mouth are not available, velocity data from KK entrance describe the circulation there between 2018 and 2022. Fig. 3d shows a persistent, near-bottom inflow of AIW into KK throughout the record, with a recurring seasonal pattern of enhanced inflow each summer and weakened flow in winter. Maximal velocities occur at the start of the observations in the summer of 2018 when speeds into the fjord reach 0.15 $\mathrm{m\,s^{-1}}$, consistent with LADCP profiles near KK2 on 22 August 2018 which yield 0.19±0.07 $\mathrm{m\,s^{-1}}$ averaged over the bottom 200 m (see also 2b, grey line and 3d, orange circle). A second pronounced period of inflow occurs in summer 2019 with a maximum velocity of 0.15 $\mathrm{m\,s^{-1}}$ in mid August. These two years stand out as the strongest summers in the record. In 2020, by contrast, the summer inflow maximum is weak and barely distinguishable from the background flow of approximately 0.06 $\mathrm{m\,s^{-1}}$, suggesting notable interannual variability in the intensity of the seasonal signal. Enhanced summer inflow resumes in 2021, reaching 0.11 $\mathrm{m\,s^{-1}}$ end of August. In 2022, the ADCP stopped recording on 7 July 2022, when velocities had increased to 0.07 $\mathrm{m\,s^{-1}}$, so the

https://doi.org/10.5194/egusphere-2026-5184
Preprint. Discussion started: 10 September 2026

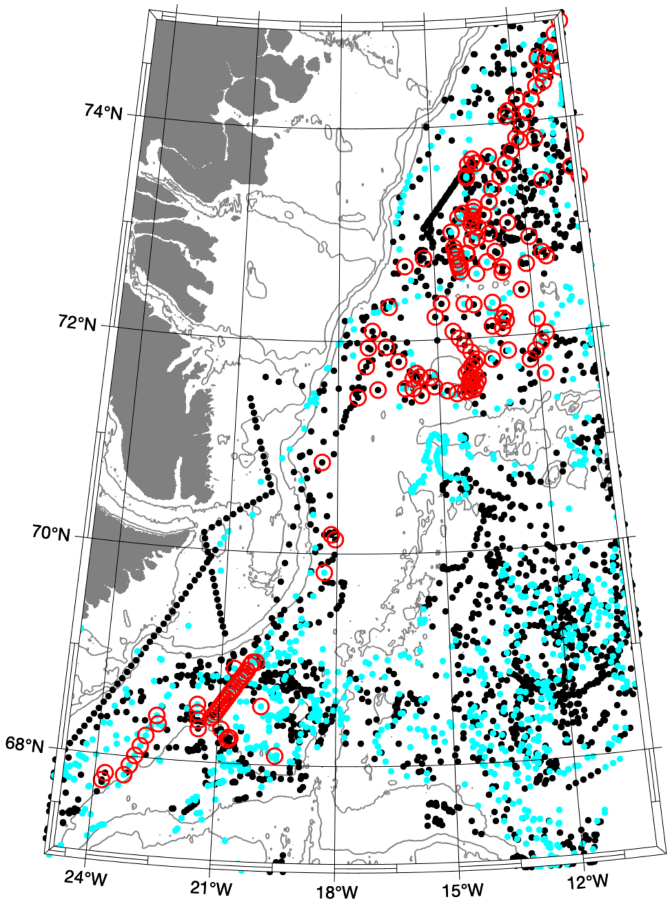

Figure 4. Position of Argo float profiles between March 2015 and March 2025. Cyan points mark winter positions (January to April) and black dots mark positions from the remaining months. Red circles show profiles containing at least one data point with salinities between 34.4 and 34.6 while temperatures are smaller than -1.0°C, corresponding to the wintertime properties at the mouth of Kangertittivaq. Depth contours of 300, 500 and 1000 m are shown as thin grey lines. The Argo data were collected and made freely available by the International Argo Program and the national programs that contribute to it (argo.ucsd.edu, ocean-ops.org) via https://dataselection.euro-argo.eu.

expected seasonal peak of maximum flow in August is not captured directly. However, LADCP observations near this mooring site on 10 August 2022 show a velocity of $0.08\pm0.06\ \mathrm{m\,s^{-1}}$ in the bottom-most 200 m, suggesting an inflow event of similar

https://doi.org/10.5194/egusphere-2026-5184
Preprint. Discussion started: 10 September 2026

magnitude to 2021. Across all years, a seasonal AIW inflow into KK emerges with velocity peaks in August that exceed 0.1 $\mathrm{m\,s^{-1}}$ in the stronger summers, while winter inflow remains generally below 0.04 $\mathrm{m\,s^{-1}}$. Although annual summer velocity maxima vary from year to year, the timing of the seasonal maxima does not vary much, suggesting regular seasonal forcing that we investigate below.

Daugaard-Jensen Glacier discharges meltwater at its base into KK, where it rises as a buoyant plume while entraining ambient fjord waters and melting the glacier. The presence of submarine melt is revealed by noble gas observations (Fig. 1d). Closest to Daugaard-Jensen Glacier we infer SMW fractions exceeding 2.6% (mean value of 1.49+/-0.54% between the surface and 150 m), and declining to just 0.15±0.09% (upper 150 m mean) toward the fjord mouth as the signal is progressively diluted. Between 2018 and 2022, the simulated entrainment of ambient AIW into the plume occurs each year between mid-May and late September, peaking at 20 mSv between 7 and 30 July, well exceeding the constant background entrainment of 5 mSv (Fig. 3d, blue line). The AIW inflow into KK lags this peak plume entrainment flux by roughly 30 days in 2019 to 2021 (Fig. 3d).

The simulated peak amplitude of the AIW entrainment flux is notably more consistent from year to year than the AIW inflow velocity is, yet the seasonal delay between the two remains stable across summers. This stable phase relationship supports the hypothesis that summertime AIW inflow events are driven by up-fjord entrainment flux caused by subglacial freshwater discharge - a mechanism consistent with classical estuarine circulation (Hansen and Rattray, 1965).

3.4 Interannual large-scale AIW variations

The FESOM2 model (Wekerle et al., 2024) simulates ocean conditions that allow us to investigate how external factors affect and drive AIW variability at Kangertittivaq (see AIW temperature distribution in Nordic Seas in Fig. 5a), reproducing the observed inflow of AIW at the northern end of the fjord mouth (S19, not shown). Correlation analysis reveals that variations in AIW temperatures occur coherently along the shelf and shelfbreak regions to the north of Kangertittivaq, and this coherent region extends all the way to Fram Strait, across it, and southward along Svalbard (Fig. 5b). We find that AIW temperatures at Kangertittivaq lag those off Svalbard by two years (Fig. 5c). Taking Svalbard as a starting point, we interpret the coherent temperature fluctuations to follow the westward recirculation and subduction pathway of Atlantic Water in Fram Strait (McPherson et al., 2023) before traveling southward along the Greenland continental slope and the path of the East Greenland Current (Håvik et al., 2017) and eventually entering the fjord, with a total transit time of approximately two years.

Independent observational evidence is consistent with this picture. Extensive aerial XCTDs deployed on the East Greenland shelf between 2016 and 2021 (Fenty et al., 2016) reveal a latitudinally coherent pattern of cooling by about 0.5°C in 2021 compared to 2018 between 70°N and 80°N (Fig. 6). Complementing this, McPherson et al. (2026) showed that the temperatures of Atlantic Water in the West Spitsbergen Current started increasing after 2013, peaked in 2016, then cooled by 1.0°C through 2019 before levelling off at lower temperatures (Fig. 7a). The AIW maximum temperature at the Kangertittivaq fjord mouth (diamonds) reveal a consistent evolution - warming by 0.5°C from 2016 to 2017 followed by equivalent cooling and reaching a low plateau after 2020. The AIW temperature at the head of KK near Daugaard-Jensen Glacier shows a warming of 0.15°C between 2016 and 2018 before cooling by 0.3°C afterwards. Despite the limited temporal resolution of these snapshot

https://doi.org/10.5194/egusphere-2026-5184
Preprint. Discussion started: 10 September 2026

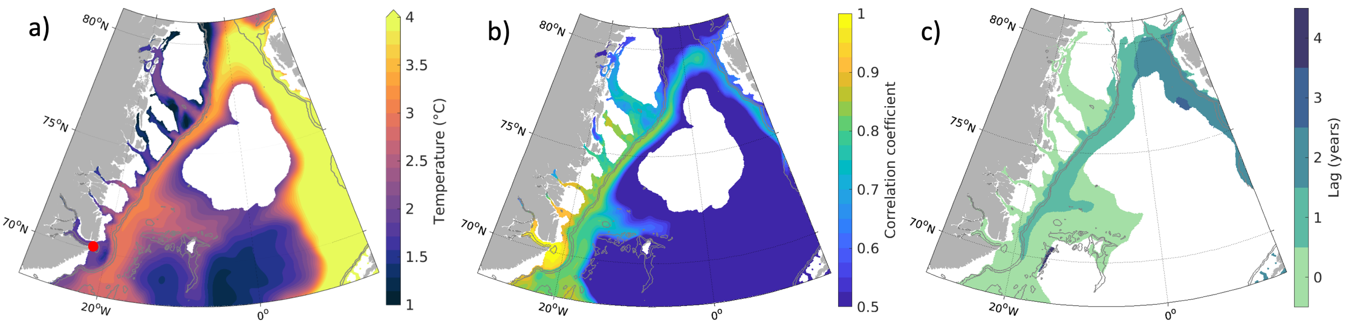

Figure 5. (a) Simulated distribution of 1970–2021 average temperature maximum (below 150 m) from FESOM2 simulation, (b) maximum of the lagged correlation of the annual mean temperature maximum at each model grid point with the simulated AIW temperatures at the mouth of Kangertittivaq (red dot), and (c) the corresponding lag in years. Only profiles with temperatures above 0°C were considered.

observations in the Kangertittivaq fjord system, the three datasets coherently reflect the same regional AIW warming-cooling
230 signal, with the amplitude progressively dampened from the mouth to the head of the fjord.

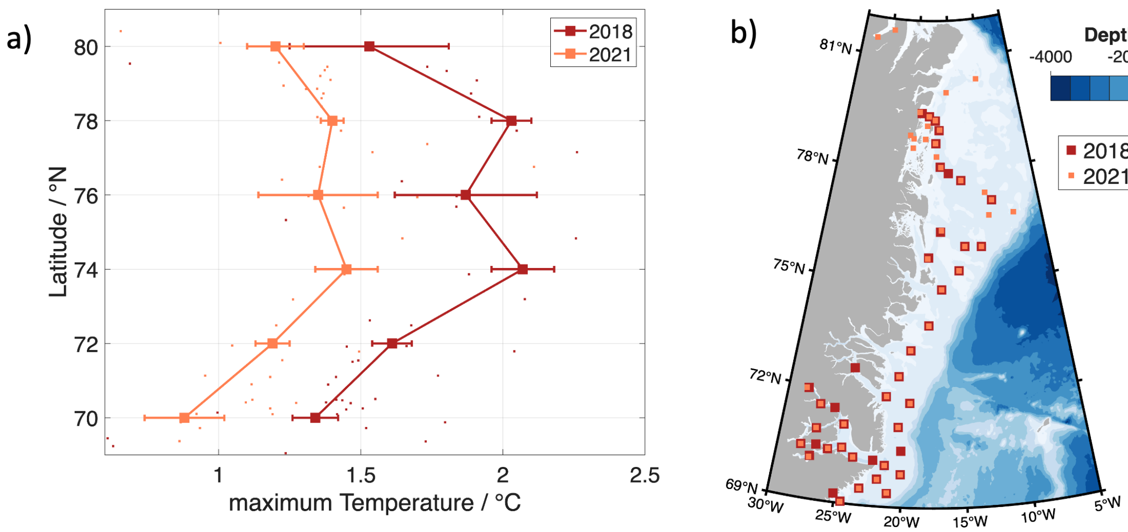

Figure 6. (a) Temperature maximum below 150 m from airborne XCTD profiles collected in 2018 (dark red) and 2021 (light red) along east Greenland between 69°N and 81°N averaged over 2° latitude intervals with standard error. Small dots are individual measurements at the corresponding latitude. (b) Map of the measurement locations.

4 Discussion and conclusions

S19 assess the link between hydrography and circulation in Greenland's largest fjord system based on snapshot observations in the summers 2016 and 2018. Our study adds a description of the temporal variability of the AIW inflow, quantifying interannual

https://doi.org/10.5194/egusphere-2026-5184
Preprint. Discussion started: 10 September 2026

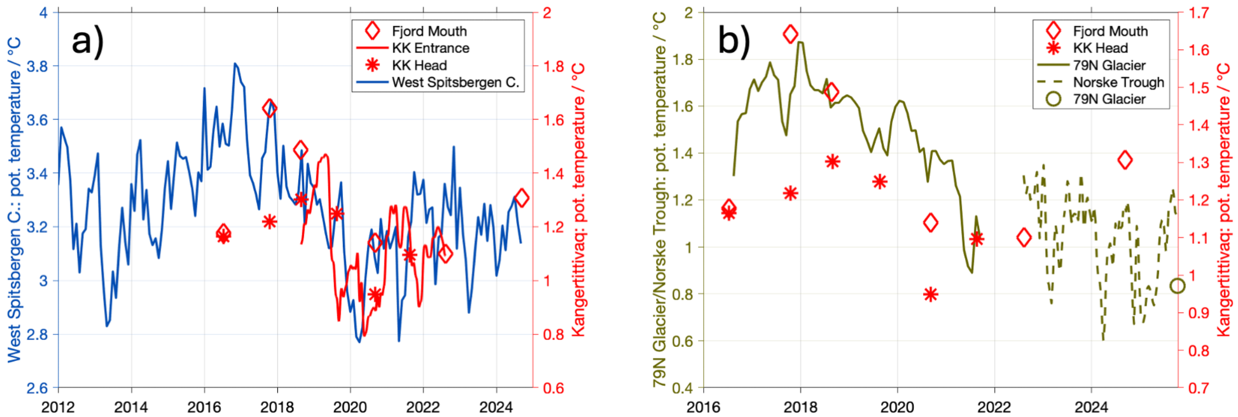

Figure 7. (a) Temperature record at 600 m from mooring KK2 (red line), 400-750 m averaged temperatures near the calving front of Daugaard-Jensen Glacier from CTD/AXCTD profiles (red asterisks), and temperature maximum at fjord mouth based on CTD profiles (diamonds). The blue line denotes mooring-based monthly mean Atlantic Water temperature in the West Spitsbergen Current (mean seasonal cycle removed; from McPherson et al. (2026)). (b) Evolution of the AIW potential temperature maximum between 2016 and 2025 near the 79N Glacier (olive) and in Kangertittivaq (red). Mooring-based time series of near-bottom AIW temperature at the calving front of 79N Glacier based on McPherson et al. (2024) (olive solid line), and of AIW temperature (interpolated onto the isopycnal surface of 27.80 kg m^{-3}) in Norske Trough roughly 100 km upstream of 79N Glacier (olive dashed line). The olive circle denotes the near-bottom AIW temperature from a CTD profile obtained at the calving front of the 79N Glacier in Oct. 2025 (Kanzow, 2026). The red diamonds and asterisks are identical to those in panel (a). All values shown represent potential temperature.

variability of AIW hydrographic properties at the fjord mouth, KK entrance, and near Daugaard-Jensen Glacier. The bottom-intensified AIW inflow of 65 mSv into KK observed in summer 2018 (S19) represents not the annual mean state, but the maximum inflow of a seasonally variable signal. Our analysis suggests the summer 2018 inflow was one of the two strongest such inflow events in the 2018 - 2022 period, with peak velocity four times larger than the 4-year average. Using the summer 2018 AIW inflow of 65 mSv as an overturning rate in KK (S19), we estimate the annual mean overturning to amount to 16 mSv. Multiplying the observed SMW fraction of 1.49 +/- 0.54% near the calving front of Daugaard Jensen Glacier by the overturning rate yields an estimated submarine meltrate of 7.5 $\pm$2.2 Gt/year occurring at the calving front.

Our results suggest that the interannual AIW cooling in Kangertittivaq originated from at least as far upstream as the West Spitsbergen Current (Figs. 5, 6, 7a). McPherson et al. (2024) noted that the recent cooling of AIW at 79N Glacier (roughly 1000 km north of Kangertittivaq) between 2018 and 2021 could likewise be traced back to an AW temperature reduction in the West Spitsbergen Current. As illustrated in Fig. 7b, the cooling pattern in Kangertittivaq parallels the AIW temperature evolution documented at the 79N Glacier over the same period. Overall, the time series suggest that during the 2022-2025 period, AIW near 79N Glacier has remained in a relatively cold state.

https://doi.org/10.5194/egusphere-2026-5184
Preprint. Discussion started: 10 September 2026

The ocean thermal forcing of glacier melt at Kangertittivaq therefore appears to follow the same basin-scale Atlantic Water variability that has been identified as a key control on melting at 79N Glacier, suggesting a common regional driver for ice-ocean interaction along this sector of the Greenland margin. Nevertheless, striking differences emerge with respect to the seasonal circulation. For the 79N Glacier, the inflow of AIW lacks a seasonal cycle (McPherson et al., 2024), whereas the inflow towards Daugaard-Jensen Glacier is strongly summer-intensified. The seasonal inflow of warm water thus represents an important mechanism of transporting heat up-fjord at Kangertittivaq. We note that a summertime development of inflows into glacial fjords driven by seasonal subglacial discharge has been found from observations in both Greenlandic as well as Alaskan fjords (Hager et al., 2022; Jackson and Straneo, 2016), with numerical model simulations suggesting it to be an important mechanism for water renewal and ocean-to-glacier heat flux. depending on fjord and glacier geometries (Carroll et al., 2017).

Our plume model indicates an AIW entrainment rate at Daugaard-Jensen Glacier that peaks at 20 mSv in summer. This value is only a third of the 65 mSv overturning obtained by S19 at KK entrance. The simulation is sensitive to parameter choices, thus several model sensitivities likely contribute to this discrepancy. First, a deeper grounding line gives higher entrainment flux because the plume has more height to rise and entrain. Second, a wider plume also gives a higher entrainment flux because the plume becomes more efficient at entraining water (see entrainment sensitivity envelope in Fig. 3d). Third, our plume model ignores large icebergs that extend into the AIW layer within KK. When such deep-reaching icebergs melt, the water upwells and drives additional entrainment of AIW. Accounting for these processes would strengthen the overall AIW entrainment rate in the fjord and bring the observed and simulated AIW entrainment rates into closer agreement. Finally, the view of a solely plume driven seasonal inflow into KK is perhaps simplistic, because forcing from the fjord entrance may heavily impact isopyncal slopes in the fjord that modulate the subsurface circulation (Mortensen et al., 2014; Jackson and Straneo, 2016). Indeed, at the fjord mouth we find the wintertime occurrence of a relatively fresh and cold water mass partly replacing the AIW. Based on wintertime observations in western Iceland Sea (Blosseville Basin) and Greenland Sea, Huang et al. (2021) find a similar water mass (absent in summer observations) originating from wintertime convection on the offshore edge of the East Greenland Current (their Fig. 12). We posit that the downward slope of the isopyncals from the offshore edge of the EGC toward the Greenland shelf break should provide a subsurface ventilation pathway for these waters toward the mouth of Kangertittivaq guided by the topographic depression across the shelf highlighted earlier (Fig. 4).

The simulation-based inference by Wood et al. (2024) that ocean-warming-driven increasing submarine melt rates triggered the retreat of the Daugaard-Jensen Glacier after 2010 should be viewed with some caution. Visual comparison of the simulated ocean warming and cooling patterns with our observations reveal agreement as well as differences in the overlapping period after 2016 - with differences occurring particularly close to Daugard Jensen Glacier, where opposing interannual trends emerge between the studies. While their highest-resolution simulation captures the observed cooling of AIW after 2018 at the fjord mouth (their Figure 2; 0.25°C, compared to roughly 0.5°C in our observations), and a sudden cooling in 2019 at the KK entrance, their simulated temperatures at the calving front show a warming of 0.3°C after 2018 - in direct disagreement with our observations. Furthermore, their highest-resolution model lacks the seasonality in the hydrographic properties that is present at KK entrance in both our observations and their coarse resolution simulation. Our data should thus be well-suited to evaluate

https://doi.org/10.5194/egusphere-2026-5184
Preprint. Discussion started: 10 September 2026

and guide detailed model simulations of ocean-glacier interactions in this fjord system. The amount of multiannual cooling of AIW we find at the fjord mouth after 2018 of O(0.5°C) is of similar amplitude as the long-term AIW warming found by Heide-Jørgensen et al. (2026) outside of Kangertittivaq (in Blosseville Basin and along the Blosseville coast) between the 1960s and 2016, demonstrating that time series spanning several decades may be required to reveal climate trends. Also, the apparent attenuation of the cooling signal from the fjord mouth towards the head of KK means that the impact of AIW temperature change on basal melt of marine terminating glaciers should be inferred from observations close to the calving front.

Overall, this study highlights the significant role of far-field Atlantic water advection in the observed cooling trends in Kangertittivaq, suggesting that external forcing is a major driver of hydrographic variability not only at the fjord mouth but throughout the entire fjord system. At KK, local seasonal forcing in summertime by glacial freshwater discharge emerges as the primary driver of the seasonal AIW inflow variability, linking large-scale ocean conditions to the delivery of heat to Daugaard-Jensen Glacier. Our results imply that coherent AIW cooling patterns and warming on the shelf of East Greenland north of Denmark Strait to originate from the Norwegian Atlantic Current-West Spitsbergen Current System. We expect there to be a different regime south of Denmark Strait, where the Irminger Current should replace the West Spitsbergen Current as main source of warm subsurface water supplied to deep southeast Greenlandic fjords.

https://doi.org/10.5194/egusphere-2026-5184
Preprint. Discussion started: 10 September 2026

Data availability. Lowered, vessel-based CTD data from the expeditions Maria S. Merian MSM 56 (Friedrichs et al., 2017), Maria S. Merian MSM 76 (Kanzow et al., 2020) and Polarstern PS131 (Hoppmann et al., 2026a) (under review) were used. In addition, aerial XCTD data from NASA's OMG program (OMG, 2016) and quality-controlled Argo float-based CTD data (Argo, 2000) were analyzed. The noble gas observations were obtained from the expeditions Maria S. Merian MSM43 (Lauvset et al., 2024) and Maria S. Merian MSM56 (Huhn et al., 2026). The LADCP (current velocity) profiles from the expeditions Maria S. Merian MSM56 (Kanzow et al., 2020) and Polarstern PS131 (Tippenhauer et al., 2023) were used. Temperature observations from AWI's long-term moorings in the West Spitsbergen Current (eastern Fram Strait) between 1997 – 2024 are based on the recent compilation by McPherson et al. (2025). Temperature, salinity and current velocity time series in Kangertittivaq were obtained from the hydrographic moorings KK1, KK2 and M (Hoppmann et al., 2023a, b, c). The temperature record from hydrographic mooring IdF in Norske Trough (near 79N Glacier) is based on Hoppmann et al. (2026b). The multi-year, mooring-based AIW temperature time series at the 79N Glacier is obtained from McPherson et al. (2024).

Author contributions. The work was conceptualized by TK. All authors contributed to the methodology. The investigation was carried out by TK, RM, CW, OH, DS and AM. TK, CW and WA led the funding acquisition. All authors contributed to writing of the original draft.

Competing interests. The authors declare there are no conflicts of interest for this manuscript.

Acknowledgements. We deeply thank the captains and crews for their support during the expeditions (listed with grant numbers) aboard R/V Maria S. Merian MSM56 (MerMet 13-15 Koch), MSM76 (GPF 18-1_1) and R/V Polarstern PS131 (AWI_PS131_07) and PS150 (AWI_PS150_01). Bathymetry data in Fig. 1c with courtesy of the Alfred Wegener Institute, Helmholtz Centre for Polar and Marine Research. We gratefully acknowledge the computing time granted by the Resource Allocation Board and provided on the supercomputer Lise at NHR@ZIB as part of the NHR infrastructure under the project hbk00099. We thank the colleagues at the Greenland Climate Research Centre and the Greenland Institute for Natural Resources in Nuuk for providing CTD data at the mouth of Kangertittivaq from a campaign in 2024. We thank Andrew Hamilton (University of Alberta) for pointing us to CTD data available in Kangertittivaq.

https://doi.org/10.5194/egusphere-2026-5184
Preprint. Discussion started: 10 September 2026

References

Argo: Argo float data and metadata from Global Data Assembly Centre (Argo GDAC), https://doi.org/10.17882/42182, 2000.

Beaird, N., Straneo, F., and Jenkins, W.: Spreading of Greenland meltwaters in the ocean revealed by noble gases, Geophysical Research Letters, 42, 7705–7713, 2015.

Carroll, D., Sutherland, D. A., Shroyer, E. L., Nash, J. D., Catania, G. A., and Stearns, L. A.: Subglacial discharge-driven renewal of tidewater glacier fjords, Journal of Geophysical Research: Oceans, 122, 6611–6629, https://doi.org/https://doi.org/10.1002/2017JC012962, 2017.

Danilov, S., Sidorenko, D., Wang, Q., and Jung, T.: The Finite-volumE Sea ice–Ocean Model (FESOM2), Geoscientific Model Development, 10, 765–789, https://doi.org/10.5194/gmd-10-765-2017, 2017.

Digby, P. S. B.: Plankton Production in Scoresby Sound, East Greenland, Journal of Animal Ecology, 22, 289–322, http://www.jstor.org/stable/1818, 1953.

Dowdeswell, J. A., Villinger, H., Whittington, R. J., and Marienfeld, P.: Iceberg scouring in Scoresby Sund and on the East Greenland continental shelf, Marine Geology, 111, 37–53, https://doi.org/10.1016/0025-3227(93)90187-z, 1993.

Dowdeswell, J. A., Batchelor, C. L., Hogan, K. A., and Schenke, H.-W.: Nordvestfjord: a major East Greenland fjord system, Geological Society, London, Memoirs, 46, 43–44, https://doi.org/10.1144/m46.40, 2016.

Fenty, I., Willis, J. K., Khazendar, A., Dinardo, S., Forsberg, R., Fukumori, I., Holland, D., Jakobsson, M., Moller, D., Moriso, J., Münchow, A., Rignot, E., Schodlock, M., Thompson, A. F., Tinto, K., Rutherford, M., and Trenholm, N.: Oceans Melting Greenland: Early Results from NASA's Ocean-Ice Mission in Greenland, Oceanography, 29, https://doi.org/10.5670/oceanog.2016.100, 2016.

Friedrichs, A., Schwalfenberg, K., Koch, B. P., and Zielinski, O.: Physical oceanography during MARIA S. MERIAN cruise MSM56 (MECAF), https://doi.org/10.1594/PANGAEA.871015, 2017.

Gjelstrup, C. V. B., Sejr, M. K., de Steur, L., Christiansen, J. S., Granskog, M. A., Koch, B. P., Møller, E. F., Winding, M. H. S., and Stedmon, C. A.: Vertical redistribution of principle water masses on the Northeast Greenland Shelf, Nat. Commun., 13, 7660, https://doi.org/10.1038/s41467-022-35413-z, 2022.

Hager, A. O., Sutherland, D. A., Amundson, J. M., Jackson, R. H., Kienholz, C., Motyka, R. J., and Nash, J. D.: Subglacial Discharge Reflux and Buoyancy Forcing Drive Seasonality in a Silled Glacial Fjord, Journal of Geophysical Research: Oceans, 127, e2021JC018 355, https://doi.org/https://doi.org/10.1029/2021JC018355, e2021JC018355 2021JC018355, 2022.

Hansen, D. V. and Rattray, M.: Gravitational circulation in straits and estuaries, J. Mar. Res., 23, 104–122, 1965.

Håvik, L., Våge, K., Pickart, R., Harden, B., Appen, W.-J. v., Jónsson, S., and Østerhus, S.: Structure and variability of the shelfbreak East Greenland Current north of Denmark Strait, Journal of Physical Oceanography, 47, 2631–2646, 2017.

Heide-Jørgensen, M. P., Chambault, P., Sørensen, H., Andresen, C. S., Ditlevsen, S., and Sun, Q.: Narwhals document atlantification of East Greenland, Science Advances, 12, eadr1424, https://doi.org/10.1126/sciadv.adr1424, 2026.

Hoppmann, M., von Appen, W.-J., Allerholt, J., Graupner, R., Kritsotalakis, S., Lochthofen, N., Monsees, M., McPherson, R., Reifenberg, S. F., and Kanzow, T.: Raw physical oceanography and ocean current velocity data from mooring SCO1-1 in Scoresby Sound, East Greenland, Aug 2018 – Aug 2022, PANGAEA, https://doi.org/10.1594/PANGAEA.964036, 2023a.

Hoppmann, M., von Appen, W.-J., Allerholt, J., Graupner, R., Kritsotalakis, S., Lochthofen, N., Monsees, M., McPherson, R., Reifenberg, S. F., and Kanzow, T.: Raw physical oceanography and ocean current velocity data from mooring SCO2-1 in Scoresby Sound, East Greenland, Aug 2018 – Aug 2022, PANGAEA, https://doi.org/10.1594/PANGAEA.964030, 2023b.

Hoppmann, M., von Appen, W.-J., Allerholt, J., Graupner, R., Kritsotalakis, S., Lochthofen, N., Monsees, M., McPherson, R., Reifenberg, S. F., and Kanzow, T.: Raw physical oceanography and ocean current velocity data from mooring SCO3-1 in Scoresby Sound, East Greenland, Aug 2018 – Aug 2022, PANGAEA, https://doi.org/10.1594/PANGAEA.964040, 2023c.

Hoppmann, M., Tippenhauer, S., Fer, I., Hofmann, Z., Mathieu, L., McPherson, R., Reifenberg, S. F., von Appen, W.-J., and Kanzow, T.: Ship CTD profiles during RV POLARSTERN cruise PS131 obtained in Scoresby Sund in August 2022, https://nextcloud.awi.de/s/j2B2T7pcqKX8g7o, dataset currently under review, 2026a.

Hoppmann, M., von Appen, W.-J., Allerholt, J., Challet, F., Eggers, N., Engicht, C., Graupner, R., Lochthofen, N., Monsees, M., McPherson, R., Mortensen, J., Münchow, A., Özkan, U., Pire, M. F., Rauschenbach, Q., Reifenberg, S. F., Rohling, C., Vernaleken, J., Wekerle, C., Welsch, A., and Kanzow, T.: Raw physical oceanography and ocean current velocity data from mooring IdF3-2 in the Greenland Sea, August 2022 – October 2025, PANGAEA, https://doi.org/10.1594/PANGAEA.993837, 2026b.

Huang, J., Pickart, R. S., Bahr, F., McRaven, L. T., and Xu, F.: Wintertime Water Mass Transformation in the Western Iceland and Greenland Seas, Journal of Geophysical Research: Oceans, 126, e2020JC016 893, https://doi.org/https://doi.org/10.1029/2020JC016893, e2020JC016893 2020JC016893, 2021.

Huhn, O., Rhein, M., Kanzow, T., Schaffer, J., and Sültenfuß, J.: Submarine meltwater from Nioghalvfjerdsbræ (79 north Glacier), northeast Greenland, Journal of Geophysical Research: Oceans, 126, e2021JC017 224, 2021.

Huhn, O., Rhein, M., and Sültenfuß, J.: Noble gas (He and Ne isotopes) measurements from RV Maria S. Merian cruise MSM56 (Scoresby Sund, East Greenland, 2016), https://doi.pangaea.de/10.1594/PANGAEA.995302, 2026.

Jackson, R. H. and Straneo, F.: Heat, Salt, and Freshwater Budgets for a Glacial Fjord in Greenland, Journal of Physical Oceanography, 46, 2735 – 2768, https://doi.org/10.1175/JPO-D-15-0134.1, 2016.

Kanzow, T.: The Expedition PS131 of the Research Vessel POLARSTERN to the Fram Strait in 2022, Tech. rep., Alfred-Wegener-Institut, Helmholtz-Zentrum für Polar- und Meeresforschung, Bremerhaven, https://doi.org/10.57738/BzPM_0770_2023, 2023.

Kanzow, T.: The Expedition PS150 of the Research Vessel POLARSTERN to the Arctic Ocean in 2025, Tech. rep., Bremerhaven, https://doi.org/10.57738/BzPM_0809_2026, 2026.

Kanzow, T., Ellmer, C., and Tippenhauer, S.: Lowered Acoustic Doppler Current Profiler (LADCP) data collected during Maria S. Merian cruise MSM76, https://doi.org/10.1594/PANGAEA.911041, 2020.

Kanzow, T., von Albedyll, L., Benz, F., Ellmer, C., Kritsotalakis, S., Lauber, J., Ali, S. M., Muchow, M., Münchow, A., Trace-Kleeberg, S., Werner, E., Wett, S., and Zippel, A.: Nordic Seas Exchanges, Cruise No. MSM 76, August 11 - September 11, 2018, Port of Sailing: Reykjavik (Iceland), Port of Arrival: Longyearbyen (Norway)., Tech. rep., https://doi.org/10.2312/cr_msm76, 2020.

Kanzow, T., Wisotzki, A., and Tippenhauer, S.: Physical oceanography during Maria S. Merian cruise MSM76, https://doi.org/10.1594/PANGAEA.910874, 2020.

Karlsson, N. B., Solgaard, A. M., Mankoff, K. D., Gillet-Chaulet, F., MacGregor, J. A., Box, J. E., Citterio, M., Colgan, W. T., Larsen, S. H., Kjeldsen, K. K., et al.: A first constraint on basal melt-water production of the Greenland ice sheet, Nature Communications, 12, 3461, 2021.

Lauvset, S. K., Lange, N., Tanhua, T., Bittig, H. C., Olsen, A., Kozyr, A., Álvarez, M., Azetsu-Scott, K., Brown, P. J., Carter, B. R., Cotrim da Cunha, L., Hoppema, M., Humphreys, M. P., Ishii, M., Jeansson, E., Murata, A., Müller, J. D., Pérez, F. F., Schirnick, C., Steinfeldt, R., Suzuki, T., Ulfsbo, A., Velo, A., Woosley, R. J., and Key, R. M.: The annual update GLODAPv2.2023: the global interior ocean biogeochemical data product, Earth System Science Data, 16, 2047–2072, https://doi.org/10.5194/essd-16-2047-2024, 2024.

Loose, B. and Jenkins, W.: The five stable noble gases are sensitive unambiguous tracers of glacial meltwater, Geophysical Research Letters, 41, 2835–2841, 2014.

Mankoff, K. D., Noël, B., Fettweis, X., Ahlstrøm, A. P., Colgan, W., Kondo, K., Langley, K., Sugiyama, S., van As, D., and Fausto, R. S.: Greenland liquid water discharge from 1958 through 2019, Earth System Science Data, 12, 2811–2841, https://doi.org/10.5194/essd-12-2811-2020, 2020a.

Mankoff, K. D., Solgaard, A., Colgan, W., Ahlstrøm, A. P., Khan, S. A., and Fausto, R. S.: Greenland Ice Sheet solid ice discharge from 1986 through March 2020, Earth System Science Data, 12, 1367–1383, https://doi.org/10.5194/essd-12-1367-2020, 2020b.

Mayer, C., Schaffer, J., Hattermann, T., Floricioiu, D., Krieger, L., Dodd, P. A., Kanzow, T., Licciulli, C., and Schannwell, C.: Large ice loss variability at Nioghalvfjerdsfjorden Glacier, Northeast-Greenland, Nature Communications, 9, https://doi.org/10.1038/s41467-018-05180-x, 2018.

McPherson, R., Wekerle, C., and Kanzow, T.: Shifts of the Recirculation Pathways in central Fram Strait drive Atlantic Intermediate Water Variability on Northeast Greenland shelf, Journal of Geophysical Research: Oceans, https://doi.org/10.1029/2023jc019915, 2023.

McPherson, R., Wekerle, C., Kanzow, T., Ionita, M., Heukamp, F., Zeising, O., and Humbert, A.: Atmospheric blocking slows ocean-driven melting of Greenland's largest glacier tongue, Science, 385, 1360–1366, https://doi.org/10.1126/science.ado5008, 2024.

McPherson, R., von Appen, W.-J., Hoppmann, M., Lochthofen, N., Monsees, M., Engicht, C., Kanzow, T., Soltwedel, T., Metfies, K., Beszczynska-Möller, A., Schauer, U., and Fahrbach, E.: Gridded hourly physical oceanography data from hydrographic moorings in the eastern Fram Strait between 1997 - 2024, https://doi.org/10.1594/PANGAEA.983454, 2025.

McPherson, R., von Appen, W.-J., de Steur, L., Kanzow, T., Beszczynska-Möller, A., and Renner, A. H.: Decades of change: Warming trends and hydrographic variability of Atlantic Water as observed in the west Spitsbergen current (1997–2024), Deep Sea Research Part II: Topical Studies in Oceanography, 227, 105 637, https://doi.org/10.1016/j.dsr2.2026.105637, 2026.

Morlighem, M. e.: IceBridge BedMachine Greenland, Version 5, https://doi.org/10.5067/GMEVBWFLWA7X, 2022.

Mortensen, J., Bendtsen, J., Lennert, K., and Rysgaard, S.: Seasonal variability of the circulation system in a west Greenland tidewater outlet glacier fjord, Godthåbsfjord (64°N), Journal of Geophysical Research: Earth Surface, 119, 2591–2603, https://doi.org/https://doi.org/10.1002/2014JF003267, 2014.

Mouginot, J., Rignot, E., Bjørk, A. A., van den Broeke, M., Millan, R., Morlighem, M., Noël, B., Scheuchl, B., and Wood, M.: Forty-six years of Greenland Ice Sheet mass balance from 1972 to 2018, Proceedings of the National Academy of Sciences, 116, 9239–9244, https://doi.org/10.1073/pnas.1904242116, 2019.

Münchow, A., Schaffer, J., and Kanzow, T.: Ocean Circulation Connecting Fram Strait to Glaciers off Northeast Greenland: Mean Flows, Topographic Rossby Waves, and Their Forcing, Journal of Physical Oceanography, 50, 509 – 530, https://doi.org/10.1175/JPO-D-19-0085.1, 2020.

OMG: OMG Airborne eXpendable Conductivity Temperature Depth (AXCTD) Profiles, https://doi.org/10.5067/OMGEV-AXCT1, 2016.

Rhein, M., Steinfeldt, R., Huhn, O., Sültenfuß, J., and Breckenfelder, T.: Greenland submarine melt water observed in the Labrador and Irminger Sea, Geophysical Research Letters, 45, 10–570, 2018.

Schaffer, J., von Appen, W.-J., Dodd, P. A., Hofstede, C., Mayer, C., de Steur, L., and Kanzow, T.: Warm water pathways toward Nioghalvfjerdsfjorden Glacier, Northeast Greenland, Journal of Geophysical Research: Oceans, 122, 4004–4020, https://doi.org/10.1002/2016JC012462, 2017.

Schaffer, J., Kanzow, T., von Appen, W., von Albedyll, L., Arndt, J., and Roberts, D. H.: Bathymetry constrains ocean heat supply to Greenland's largest glacier tongue, Nat. Geosci., 13, 227–231, https://doi.org/10.1038/s41561-019-0529-x, 2020.

Seifert, M., Hoppema, M., Burau, C., Elmer, C., Friedrichs, A., Geuer, J. K., John, U., Kanzow, T., Koch, B. P., Konrad, C., van der Jagt, H., Zielinski, O., and Iversen, M. H.: Influence of Glacial Meltwater on Summer Biogeochemical Cycles in Scoresby Sund, East Greenland, Frontiers in Marine Science, 6, https://doi.org/10.3389/fmars.2019.00412, 2019.

Slater, D. A. and Straneo, F.: Submarine melting of glaciers in Greenland amplified by atmospheric warming , Nature Geoscience, 15, 794–799, https://doi.org/10.1038/s41561-022-01035-9, 2022.

Slater, D. A., Goldberg, D. N., Nienow, P. W., and Cowton, T. R.: Scalings for Submarine Melting at Tidewater Glaciers from Buoyant Plume Theory, Journal of Physical Oceanography, 46, 1839 – 1855, https://doi.org/10.1175/JPO-D-15-0132.1, 2016.

Sültenfuß, J., Roether, W., and Rhein, M.: The Bremen mass spectrometric facility for the measurement of helium isotopes, neon, and tritium in water, Isotopes in Environmental and Health Studies, 45, 83–95, 2009.

Tippenhauer, S., Hoppmann, M., von Appen, W.-J., and Kanzow, T.: Raw data of physical oceanography during RV POLARSTERN cruise PS131, PANGAEA, https://doi.org/10.1594/PANGAEA.956136, 2023.

Tsujino, H., Urakawa, S., Nakano, H., Small, R. J., Kim, W. M., Yeager, S. G., Danabasoglu, G., Suzuki, T., Bamber, J. L., Bentsen, M., B"oning, C. W., Bozec, A., Chassignet, E. P., Curchitser, E., Boeira Dias, F., Durack, P. J., Griffies, S. M., Harada, Y., Ilicak, M., Josey, S. A., Kobayashi, C., Kobayashi, S., Komuro, Y., Large, W. G., Le Sommer, J., Marsland, S. J., Masina, S., Scheinert, M., Tomita, H., Valdivieso, M., and Yamazaki, D.: JRA-55 based surface dataset for driving ocean-sea-ice models (JRA55-do), Ocean Modelling, 130, 79–139, https://doi.org/10.1016/j.ocemod.2018.07.002, 2018.

Weiss, R. F.: Solubility of helium and neon in water and seawater, Journal of Chemical & Engineering Data, 16, 235–241, 1971.

Wekerle, C., McPherson, R., von Appen, W.-J., Wang, Q., Timmermann, R., Scholz, P., Danilov, S., Shu, Q., and Kanzow, T.: Atlantic Water warming increases melt below Northeast Greenland's last floating ice tongue, Nature Communications, 15, https://doi.org/10.1038/s41467-024-45650-z, 2024.

Wood, M., Khazendar, A., Fenty, I., Mankoff, K., Nguyen, A. T., Schulz, K., Willis, J. K., and Zhang, H.: Decadal Evolution of Ice-Ocean Interactions at a Large East Greenland Glacier Resolved at Fjord Scale With Downscaled Ocean Models and Observations, Geophysical Research Letters, 51, https://doi.org/10.1029/2023gl107983, 2024.